Time evolution of Lyman-α fine-structure components for Al XIII

J. M. A. Ashbourn*
Clare Hall, University of Cambridge, Cambridge CB3 9AL, England

I. M. Melnick and N. J. Peacock
EURATOM/UKAEA Fusion Association, Culham Science Centre, Abingdon, Oxon OX14 3DB, United Kingdom
(Received 1 October 2001; published 25 June 2002)

We present a comparison of measured and theoretically modeled Lyman-α intensity ratios of hydrogenlike Al XIII impurity ions in a deuterium base plasma in the COMPASS-*D* tokamak. The time evolution of the intensity ratios is computed from a collisional-radiative model using measured plasma parameters and compared with line-of-sight integral values measured using a high-resolution crystal spectrometer. The variations in the modeled values follow the experimental data in the case of the *L*-mode plasma, taking into account variations in the electron parameters during the discharges. Apparent discrepancies between the observed and calculated ratios in the case of the *H*-mode plasma are attributed to line blending due to satellites of nearby Fe emission.

DOI: 10.1103/PhysRevE.65.066410 PACS number(s): 52.70.−m, 32.70.Fw, 52.20.Hv, 52.25.Os

I. INTRODUCTION

The measurement of x-ray emission from excited atoms in high-temperature fusion plasmas has long been regarded as a useful plasma diagnostic, e.g., for impurity density or temperature measurement. Several papers (e.g., [1,2]) have documented comparisons between experimental Lyman-α intensity ratios with theoretical values for hydrogenlike ions in tokamak plasmas, but no consistent agreement has yet been reached. Emission lines from high-temperature ($\geqslant$1 keV) tokamak plasmas with low density ($n_e = 10^{18}-10^{20}$ m^{-3}) are invariably optically thin and broadened by mass motion and thermal motion. The use of such Lyman-α line profiles for the determination of ion temperatures from Doppler broadening requires fitting to the fine-structure components, hence reliable theoretical estimates of the Lyman-α intensity ratios are important. In this paper, we present observations from the COMPASS-*D* tokamak [3] and theoretically modeled results for the hydrogenlike ion Al XIII (ionization potential of 2299 eV) and study the time evolution of the Lyman-α intensity ratio in the tokamak plasma.

The experimental observations were made with a high-resolution ($\lambda/\Delta\lambda \sim 3000$) curved crystal spectrometer [4], which has a large area charged coupled device (CCD) detector to record spectra on a fast ($\sim$2 ms) time scale. This spectrometer has been used extensively in the study of heliumlike ions, e.g., Cl XVI [5], but in this paper we report on the use of this detection technique in the soft x-ray region to determine Lyman-α intensity ratios in a hydrogenlike ion.

Differences between the experimental and theoretical values in this study are thought to be due to the transport-linked variation in the line blending.

II. THE COMPASS-*D* TOKAMAK

COMPASS-*D* (compact assembly) is a medium-sized tokamak designed for plasma magnetohydrodynamics, shaping, confinement, and heating studies. The key parameters are shown in Table I. COMPASS-*D* is capable of achieving high confinement *H* modes in both Ohmic operation and with additional heating (electron cyclotron resonance heating) [6,7]. In the experiments reported here two deuterium plasma shots are considered: an Ohmic *H*-mode (high confinement) plasma (shot No. 16 012) and an Ohmic *L*-mode (low confinement) plasma (shot No. 16 024). Typical parameters for the two pulses are shown in Figs. 1 and 2. For shot No. 16 012, the start of the *H* mode at 125 ms and the subsequent ELM (edge localized mode) behavior [8] are shown by the D_α trace ($\lambda = 6561$ Å).

III. EXPERIMENTAL PROCEDURE

In these experiments Al was introduced into the plasma edge by laser ablation [9] and the time dependence of the Al XIII spectral lines was observed tangentially along a chord intersecting the minor axis of the torus with a curved crystal spectrometer. The Lyman-α (Ly-α) doublet lines were subsequently fitted with Voigt profiles from which the spectral

TABLE I. Parameters for the COMPASS-*D* tokamak.

Parameter	Value
Major radius	0.557 m
Minor radius (horizontal)	0.232 m
Minor radius (vertical)	0.385 m
Plasma current	100–200 kA
Toroidal field	1–2.1 T
ECRH power	2 MW at 60 GHz
LHCD power	600 kW at 1.3 GHz
Plasma duration	300–400 ms
Electron density	$8\times10^{18}-1.2\times10^{20}$ m^{-3}
$T_e(0)$ (Ohmic)	500–1000 eV
$T_i(0)$ (Ohmic)	100–400 eV

*Email address: J.M.A.Ashbourn@damtp.cam.ac.uk

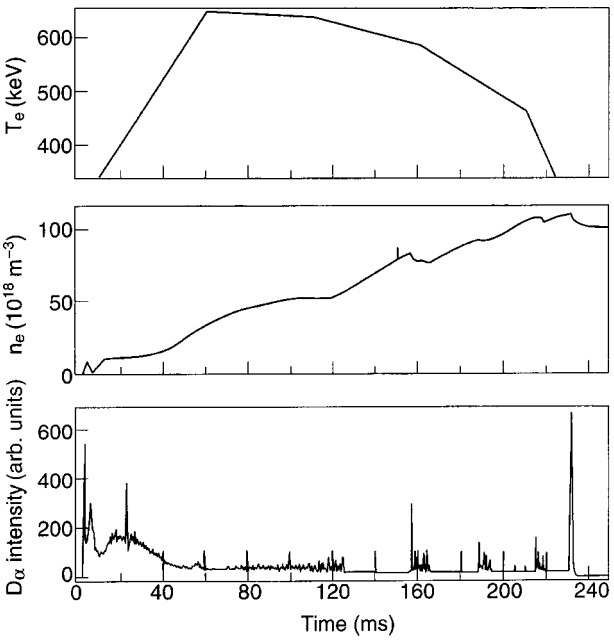

FIG. 1. Electron temperature (in eV) and density (in m^{-3}) during COMPASS-*D H*-mode pulse No. 16 012. The D_α trace (in a.u.) shows the onset of the *H* mode at 125 ms and subsequent ELM behavior. Periods of reduced D_α signal due to a reduced efflux of plasma to the walls denote periods of improved or *H*-mode confinement. These periods correspond to slight ''ramps'' in the $n_e(t)$ trace (middle graph).

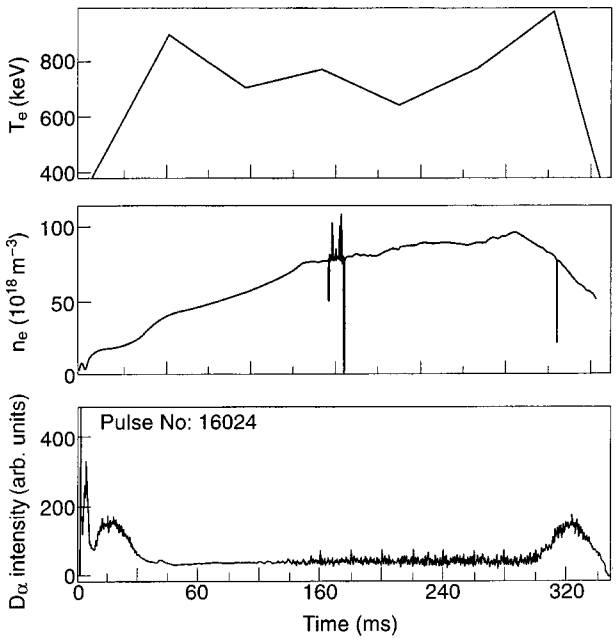

FIG. 2. Electron temperature (in eV) and density (in m^{-3}) during COMPASS-*D L*-mode pulse No. 16 024. The large spikes in the density trace are nonphysical artifacts resulting from the instrumentation and are, therefore, disregarded in the analysis.

widths and intensities were obtained.

The ion injection system consists of a laser-irradiated silicon disk coated with 5 μm or so of Al and located down a side arm of the torus vacuum vessel. The disk is placed at the focus of a ruby laser, and Al atoms, ablated from the disk by the incident laser pulse, diffuse into the plasma core on a time scale of a few milliseconds and are confined with decay time $1/e$, typically several tens of milliseconds. The *Q*-switched ruby laser ($\sim$1 J, pulse length $\sim$20 ns in duration) fires once during a plasma pulse (typically 250 ms long).

A. The spectrometer

A high-resolution Johann spectrometer, $\lambda/\Delta\lambda \approx 3000$, was used to observe the spectral lines. The design of the spectrometer allows the Bragg angle of the crystal and the Rowland circle diameter to be easily changed [10]. For this experiment, a PET (pentaerythritol) crystal, $2d = 8.742$ Å, bent to a radius of 1070 mm was used to observe the spectral region 7.11–7.22 Å. The Al Ly-$\alpha_{1,2}$ transitions are at 7.171 and 7.176 Å, respectively.

A large area CCD array was used to record the spectra [11] and consisted of 1280×1170 pixels, where the pixel size is 22.5 μm. In this experiment, the CCD was used in frame transfer mode in which half the chip is masked over and used for data storage. Charge accumulated in the exposed half is shifted and stored in a single pixel row in the frame store section of the array, which permits a time resolution of 2 ms to be achieved. Double pixels were used to reduce charge spreading. The fine-structure splitting of the lines is 5.41 mÅ [12] and corresponds to 26 double pixels, i.e., each double pixel is equivalent to 0.208 mÅ.

B. Data analysis

The spectral line profiles are distorted by two distinct phenomena. First, a line blend was found at 7.170 Å due to an intrinsic impurity ion, which, at electron temperatures greater than $\approx$700 eV, can be more intense than the transient Al lines. A number of other background lines are observed on the long wavelength side of the Al lines.

Second, due to the geometry of the vacuum system, which couples the spectrometer to the tokamak, there is vignetting at either end of the CCD chip because the x-ray path to the detector edges is obscured by the vacuum flight line. The intensity transfer function onto the chip is approximately trapezoidal. The spectral region has been chosen such that the Al lines are in the center of the detector and errors due to vignetting are thus minimized. It is estimated that the reduction in the line intensities due to vignetting is less than 4% and an example of the vignetting is shown in Fig. 3.

An approximate Voigt function [13] was used for spectral fitting in order to take account of both the instrument function, which in the absence of a measured one was assumed to be Lorentzian, and also the Doppler broadening of the lines. Three such functions were fitted to the spectra to include the Ly-α doublet and the line blend. A least-squares fitting routine was used and the value of the ''goodness of fit'' measure χ^2 for the fit was returned. Six free parameters were used for the fit, namely, three intensities, one centroid position, one line width, and the background intensity. It was found to be necessary to sum spectra from adjacent time slices together

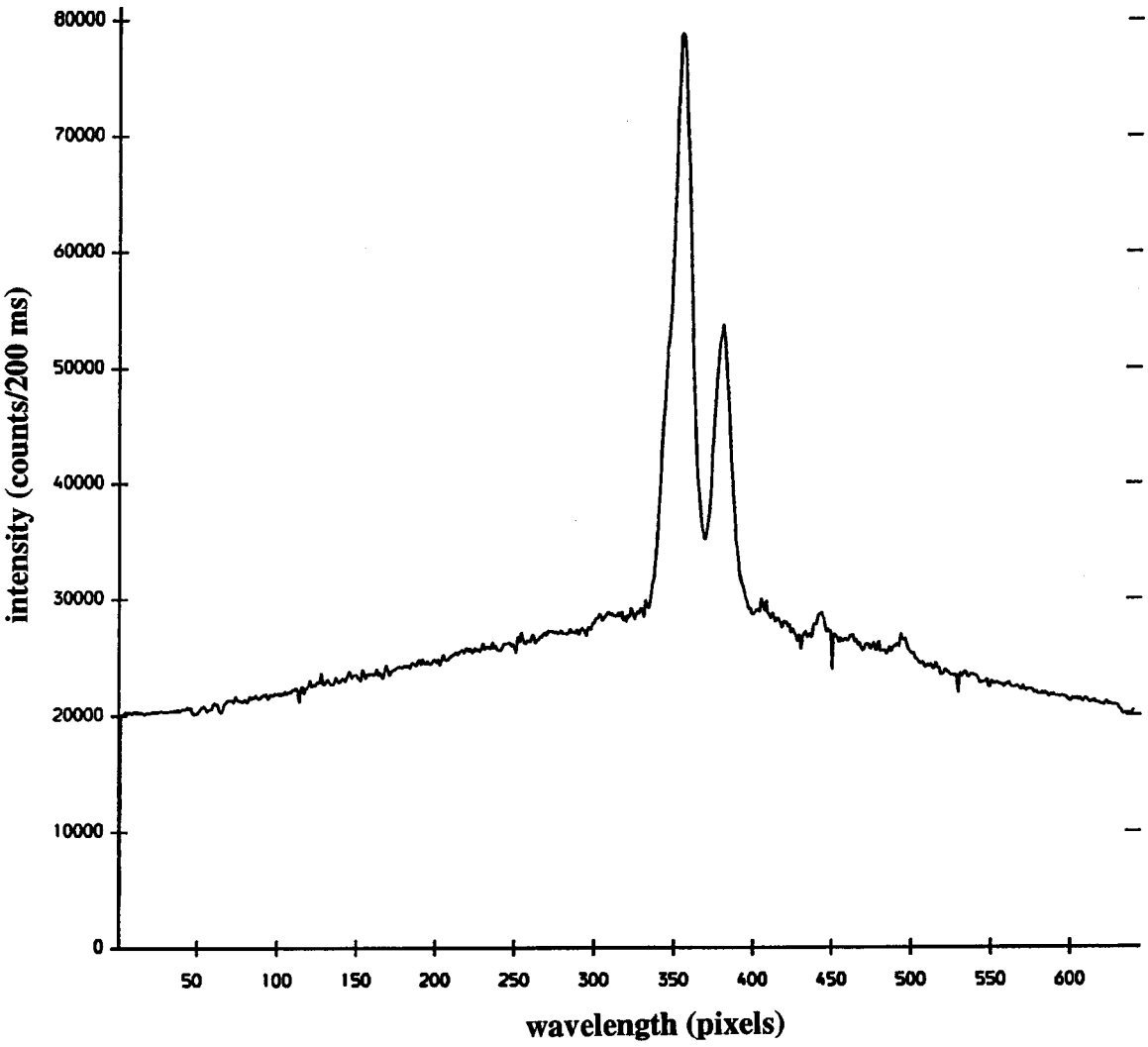

FIG. 3. Example of the vignetting with the Ly-α doublet in the "flat" region in the center.

to reduce fitting errors, and 10 ms was found to be sufficient for the spectral analysis, since increasing this resulted in no further reduction of the residuals of the fit.

A typical spectrum is presented in Fig. 4 showing the Voigt profiles fitted to the Ly-α doublet and the line blend. The residuals from the fit are shown as the wavy line about the baseline to the spectrum. The normalized value of χ^2 is 0.25 over the region of pixels from 335 to 395. Dielectronic satellite lines have not been included in the fit since at $T_e \approx 700$ eV, they are insignificant for Al ($Z=13$), i.e., a contribution to the ratio of less than 1% (as discussed in Sec. IV). The error bars on the line ratios are calculated taking into account both the estimated uncertainty due to vignetting of the profile and the uncertainty from the fit.

C. Density and temperature measurement

Density and temperature measurements are required as input to the atomic physics code COLRAD [14], which is used for the theoretical calculation of the Ly-α intensity ratios. The electron density was obtained from the COMPASS-*D* 2 mm interferometer, which provides an average density value along a vertical chord through the plasma center. The degree to which this line-average density represents the density at the location of the Al XIII emission is discussed in Sec. V. The central electron temperature values were obtained from Thomson scattering of ruby laser light, these temperature measurements being obtained at time intervals of 50 ms. In the absence of a measured instrumental width of the curved crystal spectrometer, the experimental ion temperature could not be measured directly and therefore the Artsimovich ion temperature [15] was assumed for the deuterium ions (deuterons). The Artsimovich ion temperature, which is appropriate for an Ohmically heated plasma, is based upon an energy balance of the plasma, which assumes that $1.6 \leqslant T_e/T_i \leqslant 10$, and that there is neoclassical ion energy confinement, and it is given by

$$T_i = \frac{2.8\times 10^{-6}}{A_i^{1/2}} (I_p B_\phi R^2 \overline{n_e})^{1/3} \quad (\text{in eV}), \tag{1}$$

where I_p is the plasma current, B_ϕ is the toroidal field, R is

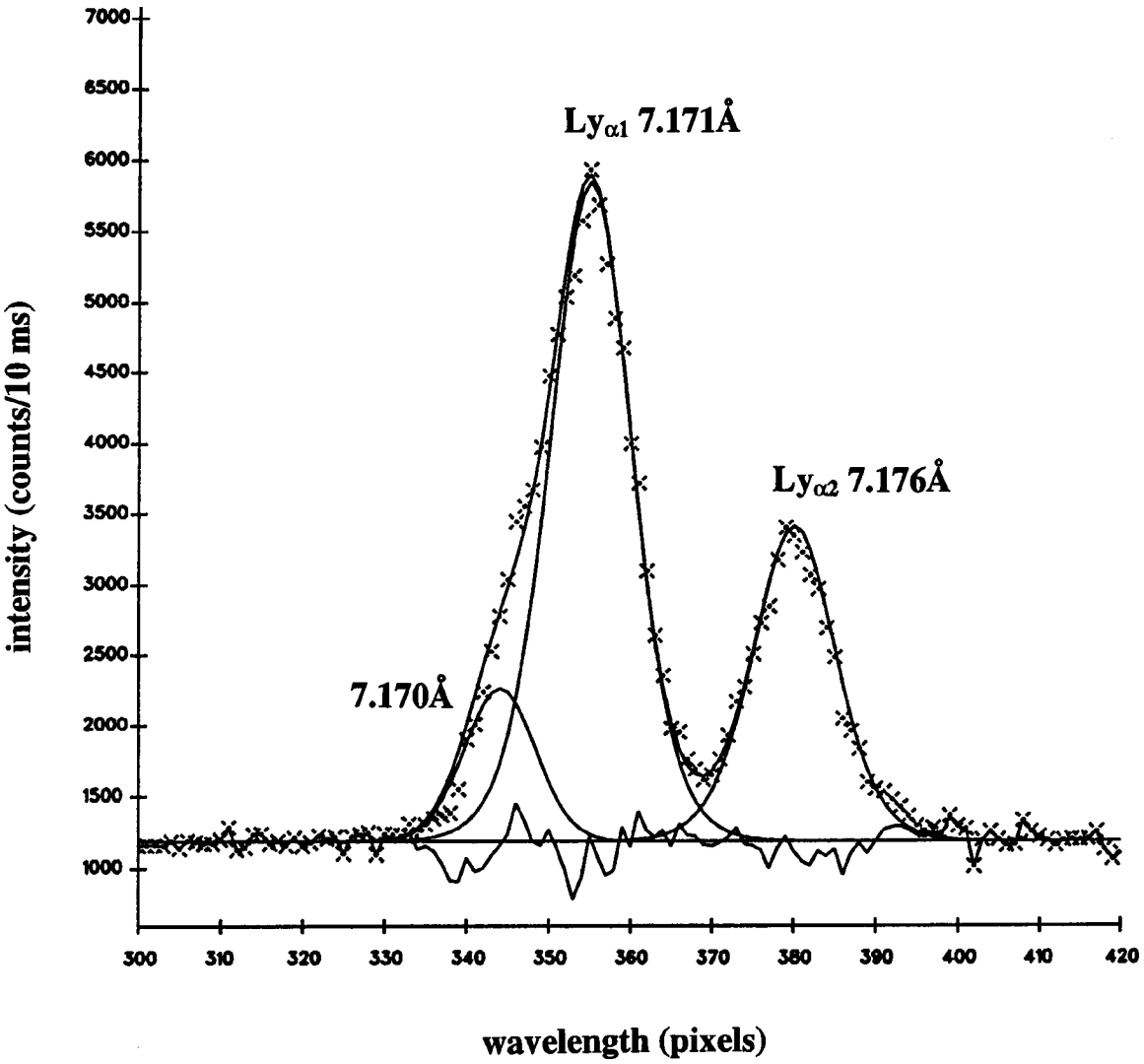

FIG. 4. Spectrum for COMPASS-*D* pulse No. 16 012, showing the Al Ly-α doublet and the line blend intensity at 7.170 Å as a function of CCD channel pairs. The residuals to the fit are shown as the wavy line about the baseline.

the major radius, $\overline{n_e}$ is the average electron density, and A_i is the ion mass. In the light of the rather weak dependence of the Ly-α ratios on the assumed T_i [see Fig. 6(a)], this is considered sufficiently accurate for this study. Impurity ion temperatures are assumed to be equal to that of the deuterium ions, as these are generally within a few tens of eV of the deuteron temperature under COMPASS-*D* conditions.

IV. THEORETICAL MODELING

In this section, we present the results of the theoretical modeling of the time evolution of the Lyman-α intensity ratios, using the experimental plasma parameters available at each time increment. We used the computer program COLRAD, which implements a collisional-radiative model to calculate the excited level populations for hydrogenlike ions and thus the intensity ratios Ly-$\alpha_{1,2}$ [16]. Modifications have been made to this program to allow for distinct ion and electron temperatures [17], whereas previous calculations performed using COLRAD had assumed the two to be equal. Multiple impurity ion species can be included in the model in addition to the background deuterium ions, with equal temperatures being assumed for the base ions and impurity ions.

The calculated intensity ratios presented here include the contribution from the magnetic dipole transition $2S_{1/2} \rightarrow 1S_{1/2}$, which cannot be resolved experimentally from the Ly-α_2 transition $2P_{1/2} \rightarrow 1S_{1/2}$, because of the small energy difference between the $2S_{1/2}$ and $2P_{1/2}$ levels. Thus the intensity ratios $\alpha_{1/2}$ and $\alpha_{3/2}$ are calculated using the sum of the contributions from the $2S_{1/2}$ and $2P_{1/2}$ states:

$$\frac{\alpha_{1/2}}{\alpha_{3/2}} = \frac{A_{(2P_{1/2}-1S_{1/2})} n(2P_{1/2}) + \mu n(2S_{1/2})}{A_{(2P_{3/2}-1S_{1/2})} n(2P_{3/2})}, \qquad (2)$$

where $A_{(2P_{1/2}\text{-}1S_{1/2})} = A_{(2P_{3/2}\text{-}1S_{1/2})}$ is the transition probability for spontaneous transitions from the $2P$ sublevels to the ground state, $n(2P_{1/2})$, $n(2S_{1/2})$, and $n(2P_{3/2})$ are the populations of the $2P_{1/2}$, $2S_{1/2}$, and $2P_{3/2}$ levels, respectively,

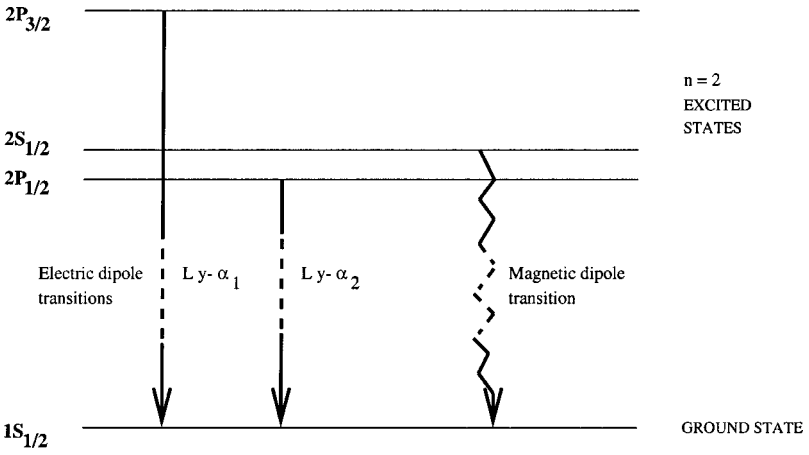

FIG. 5. Graph showing the three transitions that determine the value of the Lyman-α intensity ratio. The two straight lines represent the two optically allowed transitions, $2P_{3/2}\rightarrow 1S_{1/2}$ (Ly-α_1) and $2P_{1/2}\rightarrow 1S_{1/2}$ (Ly-α_2), while the jagged line represents the magnetic dipole transition $2S_{1/2}\rightarrow 1S_{1/2}$, which cannot be experimentally resolved from the $2P_{1/2}\rightarrow 1S_{1/2}$ transition.

and μ is the magnetic dipole transition probability for the transition $2S_{1/2}\rightarrow 1S_{1/2}$. Although the ratio of $\mu/A_{(2P_{1/2}\text{-}1S_{1/2})}$ for the transitions $2S_{1/2}\rightarrow 1S_{1/2}$ and $2P_{1/2}\rightarrow 1S_{1/2}$ is small ($\sim 1.9\times 10^{-8}$), the relative contribution of the magnetic dipole transition to the ratio is much greater (0.4% at $T_e=500$ eV, $T_i=300$ eV, and $n_e=1\times 10^{20}$ m^{-3}) due to the much larger population of the $2S_{1/2}$ level compared to that of the $2P_{1/2}$ level. The transitions contributing to the value of the intensity ratio are shown in Fig. 5.

COLRAD does not calculate the contribution to the intensity ratio from dielectronic satellite lines. However, under the density and temperature conditions considered here for COMPASS-*D*, the contribution of satellite lines to the intensities can be assumed to be negligible since the radiative decay rate (relative to the Auger rate) of the satellite lines scales as Z^4 and is, therefore, small for elements of comparatively low Z [18]. This is confirmed by an estimate of the contribution from the dielectronic satellite lines using the tables in [19], where the authors consider two bandwidths $\Delta\lambda$ centered on each component of the Lyman-α doublet: $\Delta\lambda=0.0027$ and 0.0054 Å, the latter being approximately the wavelength separation of the two doublet components. The estimated contribution to the ratio is then found to be less than 1% for both bandwidths under the temperature and density conditions for Al XIII considered in this paper.

Figures 6(a) and 6(b) show plots of the intensity ratio against electron density (for the range relevant to tokamak plasmas) for Al XIII in a deuterium base plasma, with the ion temperature varied about a constant electron temperature in Fig. 6(a), and the electron temperature varied about a constant ion temperature in Fig. 6(b). At low electron density, the intensity ratio is close to its statistical value of 0.5 since the $2P_{1/2}$ and $2P_{3/2}$ levels are populated by excitation from the ground level or by recombination and deexcitation from higher levels—both of these processes have rates proportional to the statistical weights of the $2P_{1/2}$ and $2P_{3/2}$ levels, which have similar excitation energies from the ground state. The $2S_{1/2}$ is similarly populated and decays by two-photon emission with negligible population transfer to the $2P$ sublevels at low density. As the electron density increases, the rate of collisional transfer from the $2S_{1/2}$ level to the $2P$ sublevels increases such that it matches that of two-photon decay and then actually exceeds it at sufficiently high electron density, with the result that the intensity ratio departs from its statistical value of 0.5. This is because the separation in energy is distinctly different between the $2S_{1/2}$ level and each of the $2P$ sublevels and hence there are nonstatistical collisional transfer rates for the two processes. A comparison between Figs. 6(a) and 6(b) shows that the dominant processes for the population distribution between the $2P$ sublevels are ion collisions; a change in the ion temperature at constant electron temperature has a moderate effect on the values of the intensity ratios [see Fig. 6(a)], while doubling the electron temperature from 500 eV to 1 keV at a constant ion temperature shows a much smaller effect on their values [see Fig. 6(b)]. At ion temperatures typical of COMPASS-*D* plasmas ($T_i\simeq 300$ eV), deuteron collisions are more efficient at transferring populations between the $2S_{1/2}$ and $2P_{1/2}$ levels (as $T_i/m_i\approx 1.6\Delta E_{(2S_{1/2}\text{-}2P_{1/2})}/m_e$, where m_i and m_e are the ion and electron mass, respectively) than between the $2S_{1/2}$ and $2P_{3/2}$ levels, since the $2S_{1/2}$-$2P_{3/2}$ energy separation is much larger ($\Delta E_{(2S_{1/2}\text{-}2P_{3/2})}=1.25$ eV) than that between the $2S_{1/2}$ and $2P_{1/2}$ levels ($\Delta E_{(2S_{1/2}\text{-}2P_{1/2})}=0.05$ eV). The relevant collisional rates for the impurity ions are comparatively smaller (e.g., for carbon, $T_C/m_C\approx 0.3\Delta E_{(2S_{1/2}\text{-}2P_{1/2})}/m_e$ for $2S_{1/2}$-$2P_{3/2}$). This is illustrated by calculating the change in the ratio by adding typical COMPASS-*D* impurity concentrations of 3% carbon (C^{6+}) and 0.1% iron (Fe^{16+}) (resulting in $Z_{\text{eff}}=2.14$ and $n_D/n_e=0.804$, where n_D is the deuteron density), which is found to be only 0.3% at the typical conditions of $T_e=500$ eV, $T_i=300$ eV, and $n_e=1\times 10^{20}$ m^{-3}. The influence of intrinsic impurities such as carbon is thus neglected when making comparisons between theoretical results measured values.

The Ly-α intensity ratios are calculated using COLRAD at each millisecond time increment using the measured line-average electron density, central electron temperature, and ion temperature. For both of the shots being modeled, the electron density was available at each time step (of 1 ms), but the electron temperature was only available on a 50 ms time scale, so the relevant values were obtained from a linear interpolation of the available data. Finally, the ion temperature used was that obtained from the Artsimovich scaling [15], as given by Eq. (1).

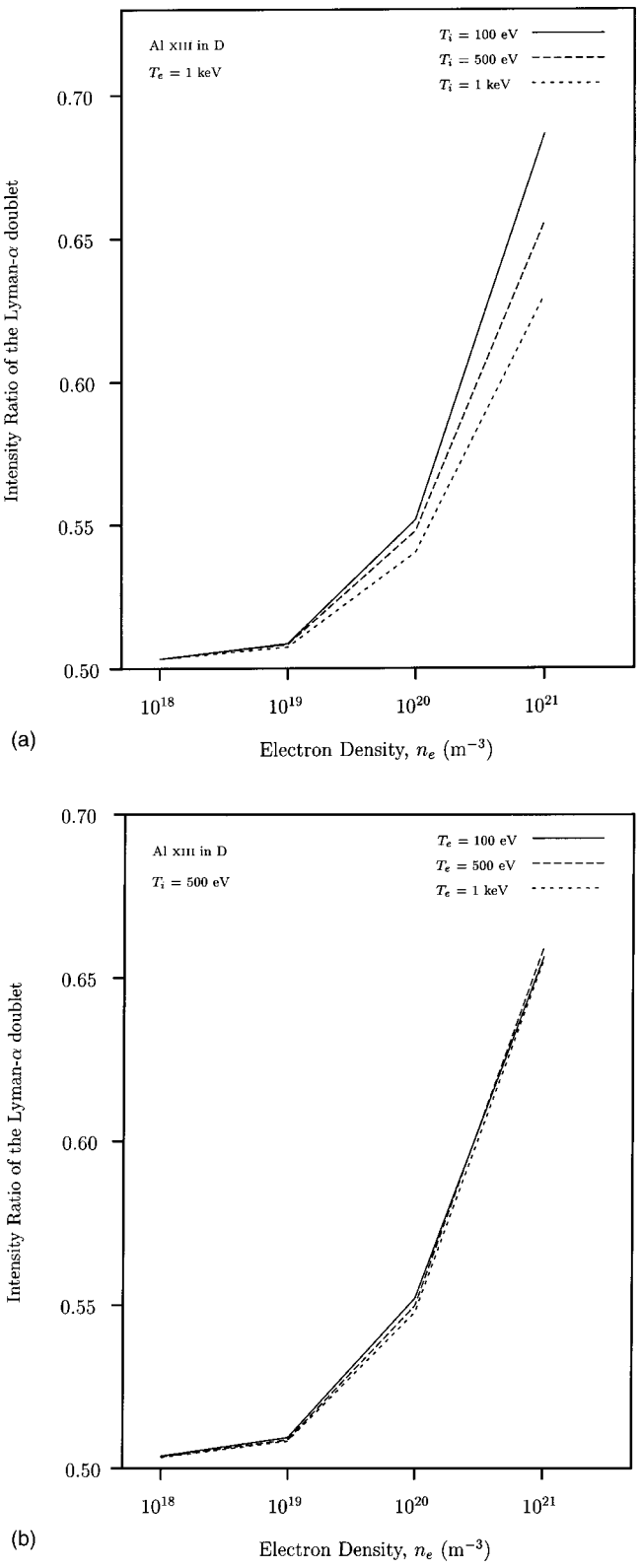

FIG. 6. (a) Plots of the calculated intensity ratios against electron density n_e (in m^{-3}) for Al XIII in a deuterium base plasma with ion temperatures T_i of 100 eV, 500 eV, and 1 keV at a constant electron temperature $T_e = 1$ keV, as shown. (b) Plots of the calculated intensity ratios against electron density n_e (in m^{-3}) for Al XIII in a deuterium base plasma with electron temperatures T_e of 100 eV, 500 eV, and 1 keV at a constant ion temperature $T_i = 500$ eV, as shown.

V. DISCUSSION

Transport simulations for the injected Al ions show the Al XIII emission profile peaks in the plasma core over the relevant range of electron densities and temperatures for the discharges considered ($5\times10^{19} \leqslant \overline{n_e} \leqslant 10^{20}$ m^{-3} and $400 \leqslant T_e \leqslant 700$ eV). The simulations were performed using STRAHL [20], a one-dimensional impurity transport code, assuming here a radially constant perpendicular diffusion coefficient $D_\perp$. The heliumlike Al XII ionization stage is most abundant in the core region, the hydrogenlike ions being typically 5–10% of the heliumlike ion concentration. These conclusions are insensitive to the assumed density profile and magnitude of $D_\perp$ over the appropriate ranges considered. Parabolic density profiles of the form $N_e \propto 1-(r/a)^m$, $m=2$ (where r is the radial coordinate and a is the minor radius), are typical of L-mode conditions with profiles during the H mode usually being flatter ($m=4$ being more appropriate). Diffusion coefficients ranging from 0.1 to 0.4 $m^2\,s^{-1}$ [21], which correspond to particle confinement times τ_p $[\sim a^2/(2.4)^2 D_\perp]$ in the range 20–70 ms, were assumed. Inward drifts such a neoclassical accumulation effects, which might occur in the H mode, would tend to cause the Al XIII density profile to peak further. As the Al XIII emission peaks in the core region, the line-averaged n_e values tend to underestimate those required for the calculation of the Ly-α ratios. For profiles of the form $1-(r/a)^m$, the ratio of peak density to line-average density is $(m+1)/m$, which is estimated to range from a modest factor of 1.25 for flatter H-mode-like profiles up to 1.5 for parabolic L-mode-like profiles. The electron temperature values used are central values and are considered appropriate, especially as the dependence of the Ly-α ratios on T_e is weak.

As the profiles of n_e were not available for these discharges, we have used the line-average n_e measurements, and consider any systematic errors due to profile effects in the following discussion. Considering first the Ohmic H-mode discharge No. 16 012, the Ly-α ratios have been calculated over the period 130–220 ms during which $\overline{n_e}$ increases overall from 6×10^{19} to 1.1×10^{20} m^{-3}, as shown in Fig. 1. During the ELM-free H mode, the particle confinement improves and n_e increases strongly. Several bursts of ELM activity cause n_e to be temporarily reduced by ~10% throughout the profile. As n_e increases, the central electron temperature decreases from 600 to 400 eV.

For the Ohmic H-mode discharge No. 16012, the calculated Ly-α ratios shown in Fig. 7 increase from 0.538 early in the H phase to 0.558 at the end of the density range. In comparison, the Ly-α ratios measured over this time interval range from 0.45 to 0.60, changing by ≈30% overall. Experimental uncertainties are typically ±7%. There is a general tendency for the calculated ratios to overestimate those measured by ≃0.05 (10%). This cannot be explained by the fact that the line-average density tends to underestimate the central value, as, if this were accounted for, the calculated Ly-α values would be still higher. While the detailed time dependence of the measured ratios does not precisely follow the calculated values, the changes in the intensity ratios occur at the times predicted by the density and confinement changes.

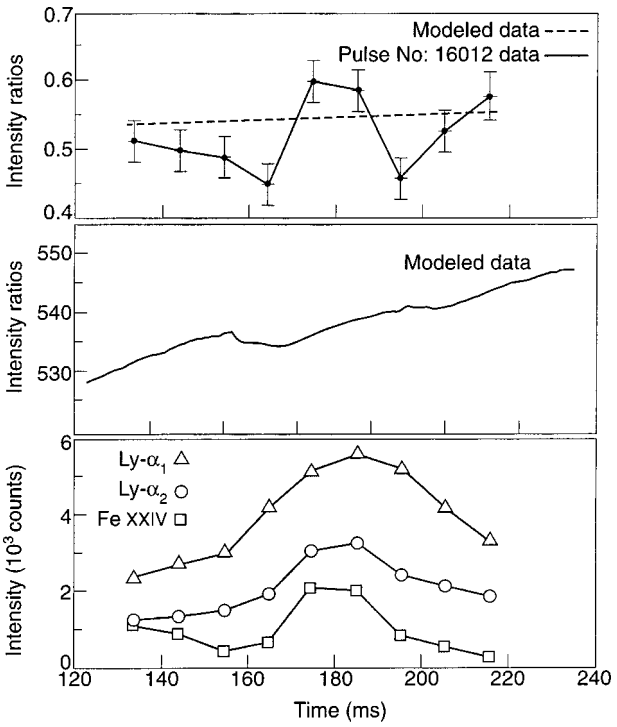

FIG. 7. The top graph shows the time evolution of both the experimental and modeled values of the intensity ratio for the *H*-mode shot No. 16 012. The middle graph shows the modeled intensity ratios on an expanded scale. The bottom graph shows the intensities of the components of the experimentally measured doublet.

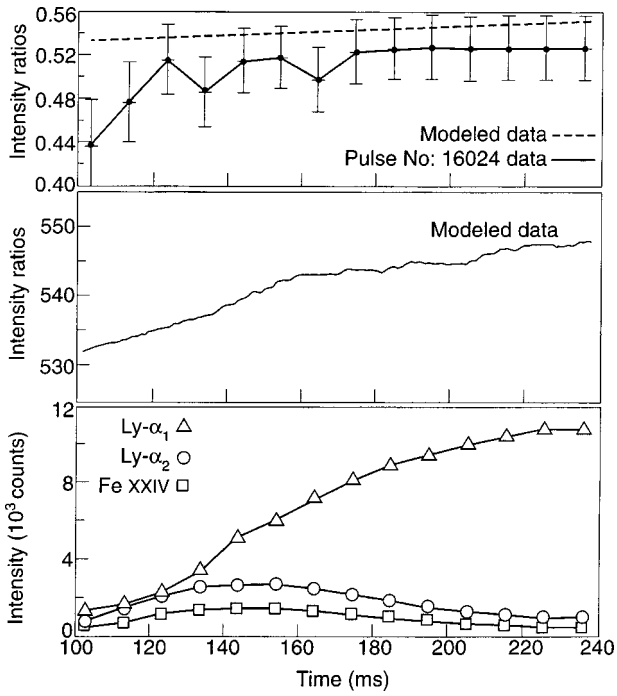

FIG. 8. The top graph shows the time evolution of both the experimental and modeled values of the intensity ratio for the *L*-mode shot No. 16 024. The middle graph shows the modeled intensity ratios on an expanded scale. The bottom graph shows the intensities of the components of the experimentally measured doublet.

The difference in measured and modeled values is probably due to a combination of systematic errors (e.g., unknown line blends) or statistical fluctuations consistent with the measurement uncertainties. The increase of 3.7% in the calculated Ly-α ratio during the *H* phase is primarily due to the increase in density by almost a factor of 2, from 6×10^{19} to 1.1×10^{20} m^{-3}. This is to be expected as the collisional coupling between the $2S_{1/2}$, $2P_{1/2}$, and $2P_{3/2}$ levels increases with density (e.g., see [16]), and hence the increased contribution to the population of the $2P_{1/2}$ level leads to an enhanced intensity ratio. The weak T_e dependence ensures that the decrease of T_e from 600 to 400 eV has little compensating influence. When a χ^2 analysis is done for this discharge, the normalized value of χ^2 (over nine data points) is found to be 3.56. However, much of this bad fit is due to two time frames at 164 and 194 ms, which denote the phase in the discharge when the confinement changes from *H* to *L* mode—during these plasma conditions the plasma pressure profile and ion transport are transients.

For the *L*-mode discharge No. 16024 shown in Fig. 8, the calculated Ly-α ratios increase from 0.532 at 100 ms to 0.544 at 240 ms. This increase of 2.2% is due to an increase in the line-average density from 5×10^{19} to 9×10^{19} m^{-3} over this period. There is little change in the measured central T_e, which remains at about 700 eV. The measured ratios increase from 0.45 to 0.52 over this period with most of this 15% increase occurring during the first 40 ms. Experimental uncertainties are typically $\pm5\%$. Again, the measured values tend to be consistently lower than those calculated by $\simeq5\%$. As for the *H*-mode discharge, using the more appropriate central electron density rather than the line-average value would only increase this discrepancy. In this case, it is more likely that an underlying systematic effect, such as an asymmetric vignetting of the measured profile, is responsible for this discrepancy. Measured ratios smaller than 0.5 are likely to be in error as processes such as heavy ion collisions influencing the intensity ratios tend to cause the ratios to exceed this value due to redistribution of populations from their statistically weighted values. This, therefore, suggests an offset systematic error due to vignetting of the order of 0.05 and hence if this is added to the experimental data, much closer agreement with the model is obtained. When a χ^2 analysis is done now for this discharge, the normalized value of χ^2 (over 14 data points) is found to be 1.23, which means that the model is a good fit to the *L*-mode data.

The model includes the contribution to the ratios from the magnetic dipole transition (as discussed in Sec. IV), but other atomic processes that are not taken into account, such as state-selective charge exchange collisions, might also have some small influence—however, these are usually much more important for neutral beam-heated plasmas rather than Ohmic plasmas as are considered here.

Line blends are an obvious complication in the intensity ratio analysis and as T_e drops below $\sim$600 eV, the errors due to the line blend (as seen from Fig. 4) begin to become significant. The strong line blend featured at 7.170 Å has been identified as being very likely due to the

Fe *XXIV* $1s^2\,2s$-$1s^2\,5p$ transition [22]; Fe is an important and common impurity in the COMPASS-*D* discharges. An estimate of the intensity of the Fe line blend calculated for COMPASS-*D* at $T_e = 900$ eV is within an order of magnitude of the Lyman-α Al XIII emission.

The intensity ratio appears in most cases to be low when the temperature is low, i.e., the line Ly-α_1 is more intense than expected. If the line blend has its own dielectronic satellites, then at low temperatures the line itself will reduce in intensity, but the dielectronic satellites will increase in intensity relative to the blend [23]. A greater proportion of the line will be due to satellites rather than due to the line itself [5], and there will be additional intense lines on the long wavelength side. Thus, these additional lines could be adding to the Ly-α_1 intensity and hence reducing the intensity ratio, since they are not accounted for in the line fitting.

Figure 7 indicates that the anomalously low values of the intensity ratio at 165 and 195 ms are coincident with the suppression of the *H* mode when transport is increased and the electron temperature drops temporarily. We postulate that these low measured values are due to the neglect of unresolved satellites of lithiumlike Fe, e.g., $1s^2\,2s^2$-$1s2s5(nl)$, etc., which lie under the Ly-α_1 line. This means that when the Fe XXIV line blend is strongest (at higher electron temperature), the intensity ratio is most secure in its accuracy.

VI. CONCLUSIONS

Measured values of the Ly-α intensity ratios tend to be systematically lower than those calculated using the COLRAD collisional-radiative model by 5–10%. Although general trends in the calculated values due primarily to density changes are observed, the measurements are insufficiently accurate to be able to make a more detailed comparison of the temporal behavior. This is due to a combination of statistical measurement uncertainties and systematic effects. The presence of a strong line blend (postulated to be from the Fe *XXIV* $1s^2\,2s$-$1s^2\,5p$ transition) accounted for in the fit and possibly other blended lines could account for observed differences in the detailed temporal evolution. Residual asymmetric vignetting of the line profile might also cause a systematic underestimate or overestimate of the ratios, since it can be difficult to decide where to assign the base continuum level—the ratio is very sensitive to the contour base level that is assumed. The spread of the Al XIII ion distribution towards the edge of the plasma in the *H* mode could, in principle, cause the intensity ratio to be characteristic of a lower density region, whereas in the *L* mode the Al XIII ions may be a central feature throughout. Bearing in mind the experimental uncertainties, the modeled Ly-α ratios do reproduce the magnitude of the measured ratios, most closely for the *L*-mode case, and also general temporal trends adequately, hence the model does replicate the variation in the experimental ratios with time—this has been shown to be true for the case where $T_e > 700$ eV in the COMPASS-*D* tokamak; however when $T_e < 700$ eV, the experimental error is too large for any firm conclusions to be reached. A more definitive test of the model requires a comparison with measurements from hydrogenlike ions with a range of charge *Z* and over a wider electron density and temperature range—in a following paper, this will be done for Cl XVII in the JET tokamak, where considerably higher temperatures, although similar densities, prevail. Finally, results from the DITE tokamak for other elements [10] have measured intensity ratios always greater than 0.5, but while the conditions for this experiment are similar to those considered here, in the DITE case, unlike for COMPASS-*D*, there are no significant problems with vignetting or line blending.

ACKNOWLEDGMENTS

The authors would like to thank Dr. N. N. Ljepojević for useful discussions, Dr. A. R. Field and Dr. P. G. Carolan for helpful comments on the draft manuscript, Dr. M. G. O'Mullane for advice on the order of magnitude intensities for the Fe line blend, Dr. R. Barnsley for assistance with the spectrometer, and finally the COMPASS-*D* team for providing the required plasma conditions. The experimental part of this work was partially funded by the UK Department of Trade and Industry and EURATOM, and part of the work done by J.M.A.A. was completed with financial funding from the Centre for Computer and Mathematical Modelling, South Bank University, London.

[1] F. Bombarda *et al.*, Phys. Rev. A **37**, 504 (1988).
[2] R. Bartiromo, F. Bombarda, and R. Giannella, Phys. Rev. A **40**, 7387 (1989).
[3] Hayward *et al.*, in *Proceedings of the 15th Symposium on Fusion Technology Utrecht*, edited by A.M. Van Ingen, A. Nijsen-Vis, and H.T. Klippel (North-Holland, Amsterdam, 1989), Vol. 1, p. 361.
[4] A. F. Abbey *et al.*, in *UV and X-Ray Spectroscopy of Laboratory and Astrophysical Plasmas*, edited by E. Silver and S. Kahn (Cambridge University Press, Cambridge, UK, 1992), p. 533.
[5] I. M. Melnick, Ph.D. thesis, University College, London, 1995.
[6] P. G. Carolan *et al.*, Plasma Phys. Controlled Fusion **36**, 116 (1994).
[7] S. J. Fielding *et al.*, Plasma Phys. Controlled Fusion **38**, 1091 (1996).
[8] H. Zohm, Plasma Phys. Controlled Fusion **38**, 105 (1996).
[9] N. J. Peacock *et al.*, in *22nd EPS Conference Proceedings, Bournemouth*, edited by B.E Keen, P.E. Stott, and J. Winter (EPS, Geneva, 1995), Vol. 19c, p. I-097.
[10] J. Dunn, Ph.D. thesis, University of Leicester, 1990.
[11] A. F. Abbey *et al.*, in *Proceedings of the 10th International Colloquium on UV and X-Ray Spectroscopy, Berkeley* (Cambridge University Press, Cambridge, UK, 1992), p. 493.
[12] P. J. Mohr, At. Data Nucl. Data Tables **29**, 453 (1983).
[13] R. D. B. Fraser and E. Suzuki, in *Spectral Analysis*, edited by J. A. Blackburn (Dekker, New York, 1970), Chap. 5.
[14] N. N. Ljepojević, R. J. Hutcheon, and J. Payne, Comput. Phys.

Commun. **44**, 157 (1987).
[15] L. A. Artsimovich, Nucl. Fusion **12**, 215 (1972).
[16] J. M. A. Ashbourn and N. N. Ljepojević, Phys. Rev. A **52**, 4966 (1995).
[17] J. M. A. Ashbourn, Phys. Rev. E **59**, 6198 (1999).
[18] J. Dubau and S. Volonté, Rep. Prog. Phys. **43**, 199 (1980).
[19] N. N. Ljepojević, R. W. P. McWhirter, and S. Volonté, J. Phys. B **18**, 3285 (1985).
[20] K. Behringer, JET Report No. JET-R(87)08, 1987 (unpublished).
[21] M. A. Singleton, Ph.D. thesis, University College, Cork, 1996.
[22] J.-F. Wyart *et al.*, Phys. Scr. **T83**, 35 (1999).
[23] F. Bely-Dubau *et al.*, Phys. Rev. A **26**, 3459 (1982).